

Temperature-dependent binding energies in a dynamical cluster-decay model applied to the decay of hot and rotating $^{56}\text{Ni}^*$

C. Karthikraj, N. S. Rajeswari, and M. Balasubramaniam*

Department of Physics, Bharathiar University, Coimbatore 641046, India

(Received 12 June 2012; published 18 July 2012)

The dynamical cluster-decay model (DCM), a nonstatistical description developed by Gupta and collaborators to account for the decay studies of excited compound nuclei formed in low-energy reactions has been applied to study various reactions. One of the main ingredients of the model is the use of temperature-dependent binding energies. In the present work, the effect of temperature-dependent binding energies in the model is analyzed. In earlier works on the DCM, the temperature-dependent liquid drop energy from Davidson *et al.*'s work [N. J. Davidson, S. S. Hsiao, J. Markram, H. G. Miller, and Y. Tzeng, *Nucl. Phys. A* **570**, 61 (1994)], with two of its constants refitted for each isotopic chain to reproduce ground-state experimental binding energies, is used. In this work, the temperature-dependent binding energy formulas of Krappe [H. J. Krappe, *Phys. Rev. C* **59**, 2640 (1999)] and Guet *et al.* [C. Guet, E. Strumberger, and M. Brack, *Phys. Lett. B* **205**, 427 (1988)] are used in the DCM without any refitting of the coefficient of the liquid drop needed to study the decay of the hot and rotating $^{56}\text{Ni}^*$ system formed in the $^{32}\text{S} + ^{24}\text{Mg}$ reaction at two incident energies, $E_{\text{c.m.}} = 51.6$ and 60.5 MeV. The use of Krappe's formula results in the explicit preference of a four-nucleon transfer, indicating a strong minima in the potential energies corresponding to α -structured nuclei as well as exhibiting structural effects in the preformation calculations favoring α -structured nuclei. The overall cross sections for the light particles and intermediate mass fragments are nicely reproduced by the use of Krappe's formula. However, the individual channel cross-sections exhibit a strong distribution only for α nuclei, and for other fragments the results are lower by a factor of 2 to 3. The use of Guet *et al.*'s formula though does not show any explicit structure effects in the potential energy calculations or the preformation calculations; the overall cross sections calculated for light particles and intermediate mass fragments compare well with the experimental data. The results of individual channel cross-sections, however, do not exhibit any explicit preference for the α -structured nuclei; rather, the individual channel cross sections decrease with an increase in the mass number of the fragments. The calculated average kinetic energies using both formulas for the favored α fragments compare well with experimental values. Without any refitting of the coefficients of the temperature-dependent binding energies, the DCM works out well and the explicit preference of α structure depends mainly on the choice of formula used.

DOI: [10.1103/PhysRevC.86.014613](https://doi.org/10.1103/PhysRevC.86.014613)

PACS number(s): 25.70.Jj, 23.70.+j, 24.10.-i, 21.10.Dr

I. INTRODUCTION

In low-energy heavy-ion collisions when two nuclei approach each other, the mutual Coulomb repulsion between them opposes the formation of a compound nucleus (CN). To overcome this, the projectiles should have larger kinetic energies to enter into the range of nuclear proximity. A CN formed in this way is in a highly excited state, carrying large angular momentum. The deexcitation and/or decay of the CN depends on the temperature and on angular-momentum-dependent potential barriers [1]. In general, the CN deexcites through the emission of light particles (LPs) with $A \leq 4$ and $Z \leq 2$ (n , p , α) and/or γ radiation. The emission of intermediate mass fragments (IMFs) and/or heavy fragments, even though suppressed, has been observed in lighter systems, $A \leq 80$ [1], formed in low-energy reactions that are always accompanied by light particle emission. For such systems, the low spin fission barriers are too high for the competition between light particle emission and fission channels.

Theoretically, different models have been employed to explain the deexcitation of a CN formed in a low-energy

heavy-ion collision. Within the dinuclear system (DNS) model concept, the fusion-fission process leading to the production of light nuclei and the characteristics of quasifission products of several reactions in different mass regions have been studied [2–4]. A full description of the DNS concept is given in Ref. [5]. Within the generalized liquid drop model and a two-center shell model Royer *et al.* [6,7] have studied the light particle emission of ^{44}Ti , ^{56}Ni , and ^{126}Ba compound systems. The statistical models like the scission point fission model [8], the saddle point transition state model (TSM) [9,10], and the extended Hauser-Feshbach model (EHFM) [11] account very well for the production of IMFs; however, the emission of LPs in these models is treated within the Hauser-Feshbach analysis only. Even though statistical fission models are able to predict the cross sections satisfactorily, extensive experimental studies have demonstrated the nonstatistical origin of the observed spectra, angular distributions of the fragments, which strongly supports a resonance phenomena [12] as an interpretation. The importance of fission mechanisms in the production of symmetric fragments has been suggested in connection with the observation of narrow resonances in excitation functions [12–14]. The equilibrium orbiting model [15,16], based on the full transport theory, accounts for the reaction data in the dinucleus complex trapped by the pocket of interaction

* m.balou@gmail.com

potential, which allows the subsequent fusion or orbiting behavior of the composite system.

The dynamical cluster-decay model (DCM), a nonstatistical description, was developed by Gupta and collaborators [17–30] to account for the emission of both light particles and intermediate and/or heavy mass fission fragments from the excited CN. Initially, within a renormalization procedure, the DCM is used to calculate decay constants (for s waves) and total kinetic energies [17,18]. Later, temperature effects [19–22] and deformation and orientation effects [23] in the model were incorporated to calculate the actual cross sections and average kinetic energies of light particles and heavy fragments. Thus far, the DCM has been applied to study different observables from several reactions [17–30].

In the DCM, the deexcitation and/or decay of a hot and rotating nucleus has been understood as a collective clusterization process. Moreover, in this model the light particle emission and the intermediate and/or heavy fragment emission are treated as the dynamical mass motion of preformed clusters passing the interaction barrier. Since, the deexcitation of fragments are treated within the cluster-decay process, the structural effects enter the model via the preformation of the fragments.

One of the main ingredients of the DCM is the use of temperature (T)-dependent binding energies. Thus far, the T -dependent liquid drop model (LDM) energy of Davidson *et al.*, [31] along with the Myers-Swiatecki shell corrections [32], has been used within a Strutinsky procedure. However, the liquid drop part of Davidson *et al.*'s formula [31] was refitted for two of its constants (for each isotopic chain), viz., the bulk constant associated with the volume term and the proton-neutron asymmetry constant so as to give the ground state (at $T = 0$ MeV) experimental binding energies [17,19,23]. The mass excess values calculated from the temperature-dependent liquid drop binding energy of Davidson *et al.* [31] were used to calculate the temperature-dependent fragmentation potentials. In the present work to study the effect of temperature-dependent binding energies in the DCM two different forms of temperature-dependent binding energies calculated using Krappe's formula [33] and Guet *et al.*'s formula [34] are used.

In Guet *et al.*'s formula [34], the temperature dependence of the coefficients in a liquid drop model type expansion of the free energy of a hot nucleus is determined by using the extended Thomas-Fermi density functional approach [35,36]. In Krappe's formula [33], the Gibbs free energy of hot, finite nuclei is described by generalizing the Yukawa plus exponential mass formula [37] and the temperature dependence of the coefficients is obtained by fitting the results of temperature-dependent Thomas Fermi calculations. Since Guet *et al.*'s formula [34] is proposed to give the T dependence of the leading LDM and droplet model coefficients it does not have terms like pairing and Wigner terms. However, in Krappe's formula [33], in addition to the liquid drop energy proper, the temperature dependence of the pairing and Wigner terms are also given. However, in the present calculations the temperature effects in pairing and Wigner terms are not considered.

In the present calculations no refitting of the coefficients was done; rather the actual form of the expressions given in Refs. [33,34] are used. In both formulas, the empirical

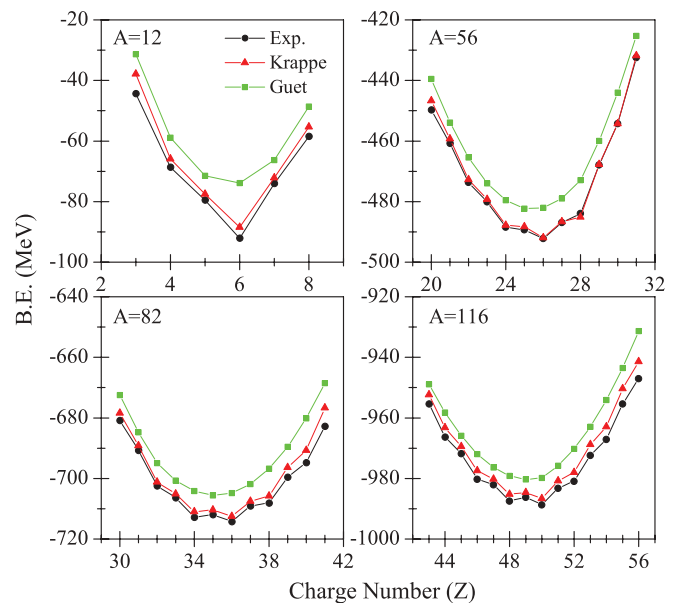


FIG. 1. (Color online) Ground-state binding energies (at $T = 0$ MeV) calculated using Krappe's formula and Guet *et al.*'s, formula are compared with experimental values [38] of some representative isobars with mass numbers $A = 12, 56, 82,$ and 116 .

shell corrections of Myers and Swiatecki [32] are added so as to reproduce the ground-state experimental binding energies [38]. However, at the temperatures that interest us these shell corrections are considered to vanish exponentially as given in Eq. (13) of Ref. [21]. Krappe's formula, without any refitting of the constants, reproduces the experimental ground-state binding energies as presented in Fig. 1 for some representative isobars with mass numbers $A = 12, 56, 82,$ and 116 . In this figure, the solid circles correspond to the experimental values, the solid triangles are the values calculated using Krappe's formula, and the solid squares are the results obtained from Guet *et al.*'s formula. The Guet *et al.* formula gives the shape of the mass parabola, but it does not compare well with the experimental binding energies as is evident from this figure. As stated earlier this may be due to the noninclusion of terms like pairing and Wigner terms. Though these terms are important to reproduce the ground-state binding energies, they may not play a crucial role if the temperature effects are considered. At the temperatures that interest us, the contribution of these terms will be negligible and the structural effect present, if any, will be due to the liquid drop terms only.

Though no refitting of the constants is done, the contribution of the Wigner term in Krappe's formula is considered only for nuclei with $A > 11$. For $A < 12$, the inclusion of the Wigner term resulted in a larger deviation with respect to experimental binding energies and hence the contribution due to the Wigner term is not considered for $A < 12$. The results for the isobars with mass numbers $A = 4$ to 11 are presented in Fig. 2.

In the present work, the role of temperature-dependent binding energies calculated using Krappe's formula and Guet *et al.*'s formula in the DCM is studied for the deexcitation of $^{56}\text{Ni}^*$ formed in the $^{32}\text{S} + ^{24}\text{Mg}$ reaction at two different incident energies. In the $^{32}\text{S} + ^{24}\text{Mg}$ reaction, the primary,

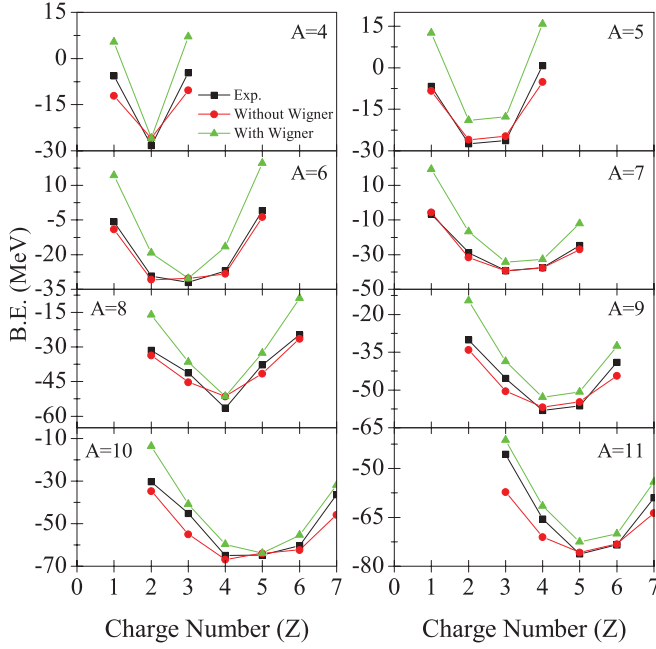


FIG. 2. (Color online) Ground-state binding energies calculated using Krappe's formula with and without the inclusion of Wigner term are compared with the experimental values for nuclei with mass numbers $A = 4$ to 11 .

pre-evaporation mass distribution, prior to secondary light particle emission, is measured using coincident detection at two incident energies, viz., $E_{\text{lab}} = 121.1$ and 141.8 MeV corresponding to the center of mass energy of $E_{\text{c.m.}} = 51.6$ and 60.5 MeV [9]. The fragment masses, through momentum conservation, were measured for the four-nucleon fragments $A = 12$ to 28 . For the incident energy $E_{\text{c.m.}} = 51.6$ MeV only even- A fragments were measured. Also, the mass-asymmetric breakup of the compound system is favored over symmetric fission. The average total kinetic energies TKE for α fragments were also measured in this experiment. The fission channel cross section estimated in one of these experiments is 59 ± 12 mb. The CN fusion cross sections due to multiple pre-evaporations at these energies are also measured; they are 1080 ± 130 and 1050 ± 100 mb, respectively, at $E_{\text{c.m.}} = 51.6$ and 60.5 MeV.

The paper is organized as follows. The DCM is explained in Sec. II for the use of two temperature-dependent binding energy formulas. Results obtained from both the T -dependent forms for the reaction $^{32}\text{S} + ^{24}\text{Mg}$ formed at two incident energies are discussed in detail in Sec. III. Finally, a summary of the results is presented in Sec. IV.

II. THE METHODOLOGY

The collective coordinates of the DCM are the relative separation R between the centers of the two fragments and the mass (and charge) asymmetry given as

$$\eta = \frac{(A_1 - A_2)}{(A_1 + A_2)}; \quad \eta_z = \frac{(Z_1 - Z_2)}{(Z_1 + Z_2)}, \quad (1)$$

(where 1 and 2 refer to heavy and light fragments, respectively). The temperature-dependent fragmentation potential $V(\eta)$ at a fixed R is given by

$$V(\eta, T, \ell) = - \sum_{i=1}^2 [BE_{\text{LDM}}(A_i, Z_i, T)] + \sum_{i=1}^2 \delta U_i(T) + \frac{Z_1 Z_2 e^2}{R(T)} + V_P(T) + \frac{\hbar^2 \ell(\ell + 1)}{2I_S(T)}, \quad (2)$$

where $e^2 = 1.44$ MeV fm and $R(T)$ is the relative separation distance between the centers of the fragments and at touching denoted as $R_t(T) = R_1(T) + R_2(T)$ with the radius expression defined as in Ref. [33] as

$$R_i(T) = 1.16(1 + 7.63 \times 10^{-4} T^2) A_i^{1/3} \text{ fm}. \quad (3)$$

Here $i = 1$ and 2 correspond to the heavy and light fragments, respectively. (It should be mentioned that, in our earlier works regarding the use of Davidson *et al.*'s [31] formula, the radius expression used is as given in Refs. [18,31], with radius R having a linear dependence on temperature T .) Whenever two nuclei are closer to each other an additional attraction will contribute to the total energy; for this additional attraction the nuclear proximity potential of Blocki *et al.* [39] is used and is defined as

$$V_P(T) = 4\pi \bar{R}(T) \gamma b(T) \Phi[s(T)], \quad (4)$$

with $\bar{R}(T) = \frac{R_1(T)R_2(T)}{R_t(T)}$ defining the inverse of the root mean square radius of the Gaussian curvature. $\Phi[s(T)]$ and γ are universal functions independent of the geometry of the system and the nuclear surface energy coefficient, respectively (See Eqs. (17) and (18) of Ref. [21]), with

$$s(T) = \frac{R(T) - [R_1(T) + R_2(T)]}{b(T)} \quad (5)$$

being the separation distance between the two surfaces in units of $b(T)$, which is defined in Ref. [33] as

$$b(T) = 0.68(1 + 7.37 \times 10^{-3} T^2) \text{ fm}. \quad (6)$$

The moment of inertia in the complete sticking limit is

$$I_S(T) = \mu R_t^2(T) + \frac{2}{5} A_1 m R_1^2(T) + \frac{2}{5} A_2 m R_2^2(T). \quad (7)$$

Here $\mu = [A_1 A_2 / (A_1 + A_2)] m$ is the reduced mass with m as the nucleon mass.

Using the fragmentation potential defined in Eq. (2), the solution of the following stationary Schrödinger equation,

$$\left\{ - \frac{\hbar^2}{2\sqrt{B_{\eta\eta}}} \frac{\partial}{\partial \eta} \frac{1}{\sqrt{B_{\eta\eta}}} \frac{\partial}{\partial \eta} + V_R(\eta, T) \right\} \psi^v(\eta) = E^v \psi^v(\eta), \quad (8)$$

after normalization would give the the preformation probability as

$$P_0(A_i) = |\psi[\eta(A_i)]|^2 \sqrt{B_{\eta\eta}} \frac{2}{A}. \quad (9)$$

The mass parameters $B_{\eta\eta}(\eta)$, representing the kinetic energy part in Eq. (9), are the smooth classical hydrodynamical

masses [40]. The temperature dependence of preformation probability is calculated as

$$|\psi|^2 = \sum_{\nu=0}^{\infty} |\psi^{\nu}|^2 \exp(-E^{\nu}/T). \quad (10)$$

For R coordinate motion, at a fixed η , the WKB approximation is used to find the barrier penetration probability between the two turning points R_a and R_b as

$$P = \exp \left[-\frac{2}{\hbar} \int_{R_a}^{R_b} \{2\mu[V(R) - Q_{\text{eff}}]\}^{1/2} dR \right]. \quad (11)$$

The T -dependent scattering potential $V(R)$ in Eq. (11) is the sum of the last three terms in Eq. (2). For the decay of the CN, as suggested in Refs. [17–19], the first turning point $R_a(T)$ is considered to be

$$R_a(T) = R_t(T) + \Delta R(T), \quad (12)$$

with the corresponding potential $V(R_a)$ acting as an effective Q value, Q_{eff} , and R_b as the second turning point satisfying

$$V(R_a) = V(R_b) = Q_{\text{eff}} = \text{TKE}(T). \quad (13)$$

Here, $\Delta R(T)$ is the only free parameter (to fit the experimental data) of the model that is allowed to vary between 0.1 and 1.5 fm where the proximity forces are said to exist. $\text{TKE}(T)$ refers to the total kinetic energy, with the available CN excitation energy shared as

$$E_{\text{CN}}^* = |Q_{\text{out}}(T)| + \text{TKE}(T) + \text{TXE}(T). \quad (14)$$

The excitation energy of the CN for the deexcitation is due to the sum of the entrance channel center of mass energy $E_{\text{c.m.}}$ and the Q value, Q_{in} , for the incoming channel. For the calculation of Q_{in} , we use the experimental binding energies [38]. $\text{TXE}(T)$ is the excitation energy carried by the emitted fragments that will be shed by the secondary particle emission, which, however, is not treated in the model. In the DCM, the decay cross section [18,19] is defined as

$$\sigma = \sum_{\ell=0}^{\ell_{\text{max}}} \sigma_{\ell} = \frac{\pi}{k^2} \sum_{\ell=0}^{\ell_{\text{max}}} (2\ell + 1) P_0 P; k = \sqrt{\frac{2\mu E_{\text{c.m.}}}{\hbar^2}}, \quad (15)$$

with ℓ_{max} taken as the ℓ value where the light particle cross section $\sigma_{\text{LP}} \rightarrow 0$. The value of ℓ could also be taken as a variable parameter to fit the experimental data; however, this is not attempted here.

III. RESULTS AND DISCUSSION

The fragmentation potential as defined in Eq. (2) (at $R = R_t$ and $\ell = 0\hbar$) for the fragmentation of $^{56}\text{Ni}^*$ formed in the reaction $^{32}\text{S} + ^{24}\text{Mg}$ at $T = 0$ MeV is presented in Fig. 3 as a function of the fragment mass number A_2 . The solid line corresponds to the use of ground-state experimental binding energies [38]. Dashed and dotted lines correspond to the use of Krappé's and Guet *et al.*'s binding energies, respectively. The results due to experimental binding energies clearly exhibit strong minima at α nuclei indicating a four-nucleon transfer of the mass asymmetry coordinate η .

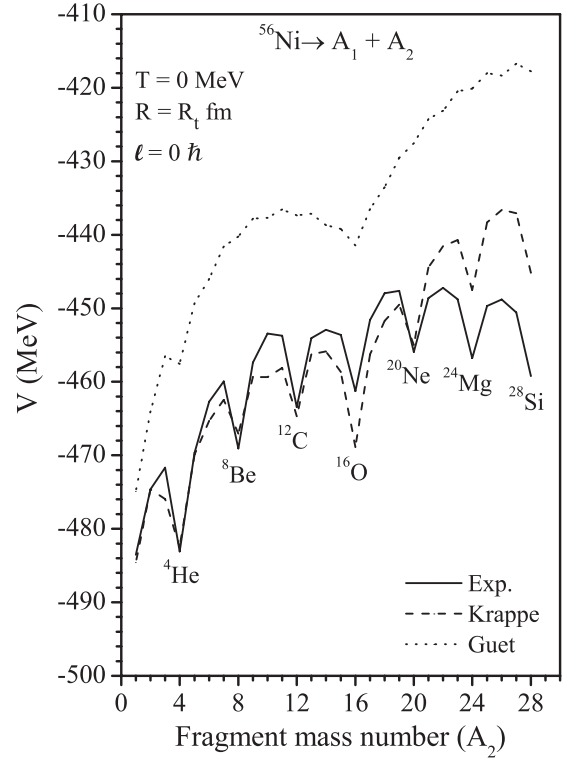


FIG. 3. The fragmentation potential of ^{56}Ni at $T = 0$ MeV, $R = R_t$, and $\ell = 0\hbar$. The solid line corresponds to the use of experimental binding energies [38] and the dashed and dotted lines correspond to the use of binding energies calculated using Krappé's formula and Guet *et al.*'s, formula, respectively. The α -structured nuclei are labeled.

The calculations obtained with Krappé's formula have a structure similar to that of the results due to experimental binding energies. Strong minima are present for α nuclei. However, the calculations obtained using Guet *et al.*'s formula do not show any strong minima in the potential; rather a small minima is present at ^4He and ^{16}O . As mentioned earlier, Guet *et al.*'s formula without any refitting done to reproduce the ground-state experimental binding energies has a larger deviation due to the noninclusion of terms like the Wigner term, pairing, and other microscopic correction terms. The potential more or less depicts the shell structure present at ^4He and ^{16}O . Odd-even structure is also not strongly present in this calculation. However, this potential at $T = 0$ MeV does not enter into any calculations. The temperature-dependent fragmentation potential as a function of the fragment mass number A_2 and the angular momentum ℓ is presented in Figs. 4 and 5 for Krappé's formula and Guet *et al.*'s formula. In these figures the potentials are plotted at $R = R_t$ fm and $T = 3.3272$ MeV, corresponding to the center of mass energy $E_{\text{c.m.}} = 51.6$ MeV. In Fig. 4, even with the temperature included, the potential energy retains the favored α -nuclei structure, exhibiting strong minima at the α nuclei. This structure remains for higher angular momentum values as well. In Fig. 5, using Guet *et al.*'s formula, the preferred α structure is not present, rather only an odd-even structure is present for all the angular momentum states considered. It should be mentioned here that, in earlier works by one of us [21], when

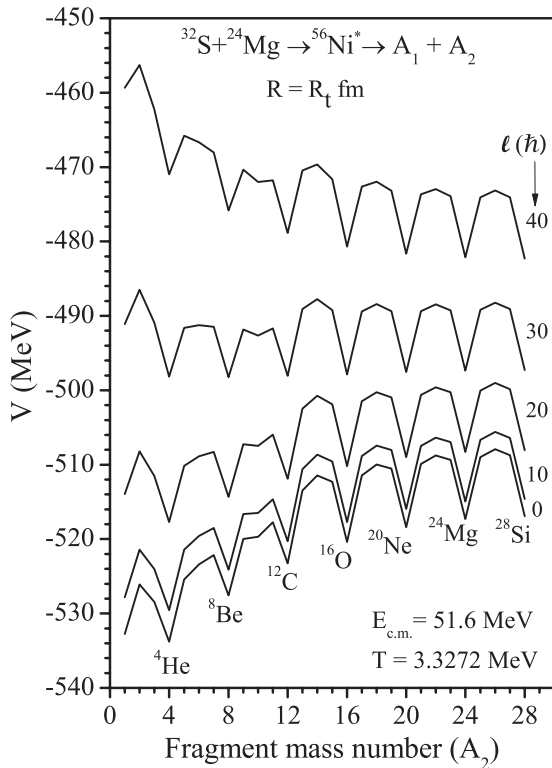


FIG. 4. The fragmentation potential of $^{56}\text{Ni}^*$ obtained using Krappe's formula at $T = 3.3272$ MeV as a function of the fragment mass number (A_2) and the angular momentum. Strong minima are seen at the α -structured nuclei.

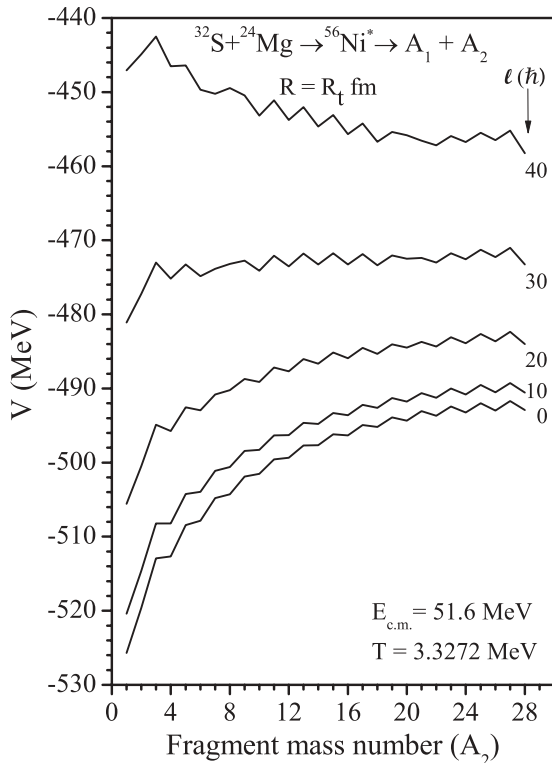


FIG. 5. Same as Fig. 4 but for binding energies obtained using Guet *et al.*'s formula. The α -structured nuclei are not showing strong minima, rather an odd-even effect is present in the potential.

Davidson *et al.*'s formula [31] was used, the potential had only an odd-even structure and there was no explicit preference for the α -structured nuclei, and it was interpreted that with the inclusion of temperature not only the shell effects vanish but also the explicitly preferred α -nucleus structure also vanishes. However, from the present study it is inferred that the form of the temperature-dependent binding energies determines the presence of the shell effect and/or the α -nucleus structure as is evident from Figs. 4 and 5.

However, in all three calculations, the preference of asymmetric channels over symmetric channels in low angular momentum states and the preference of symmetric channels over asymmetric channels at higher angular momentum states are seen. The effect of strong minima in the potential energy curve is reflected in the calculations of preformation probability and in turn in the cross-section calculations. Similar results are seen for another temperature, $T = 3.5405$ MeV; however, these are not presented here.

In Fig. 6, the preformation probabilities (P_0) as a function of angular momentum (ℓ) and fragment mass number (A_2) are presented in the upper (a) and lower (b) panels corresponding to Krappe's formula and Guet *et al.*'s formula, respectively, for the temperature $T = 3.3272$ MeV. For the light particles, the touching configuration is extended by the free parameter ΔR taking a value of 1.11 and 0.88 fm corresponding to Krappe's formula and Guet *et al.*'s formula, respectively, so

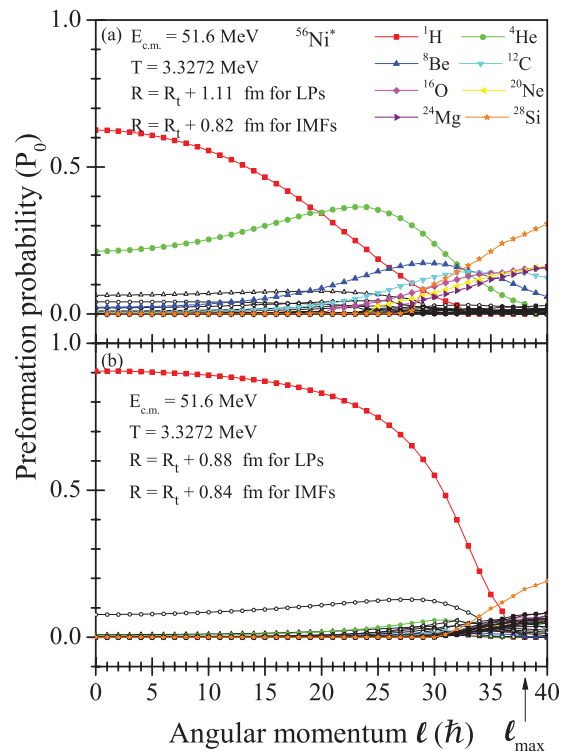


FIG. 6. (Color online) The fragment preformation probability (P_0) as a function of angular momentum ℓ for the $^{56}\text{Ni}^*$ compound system is calculated by both Krappe's formula (a) and Guet *et al.*'s formula (b) at $T = 3.3272$ MeV and $E_{\text{c.m.}} = 51.6$. Here the P_0 values for LPs and IMFs are plotted for fitted ΔR values. The α -structured nuclei are strongly favored.

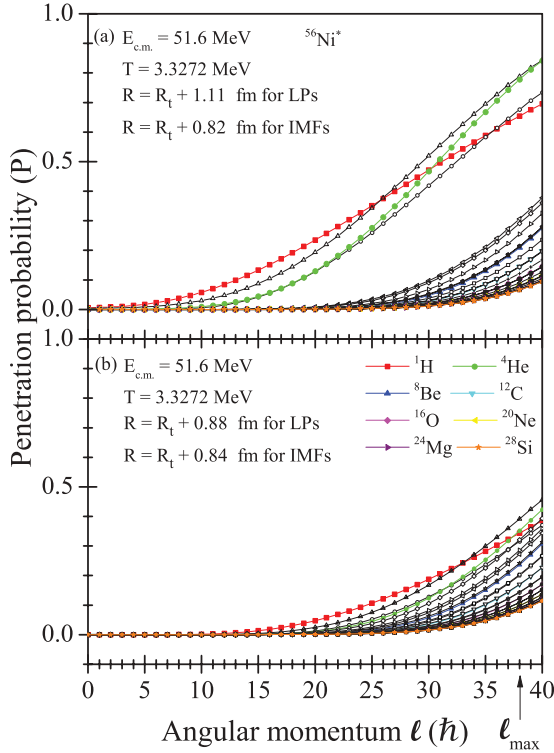


FIG. 7. (Color online) The fragment penetration probability P as a function of angular momentum ℓ for the $^{56}\text{Ni}^*$ compound system is calculated by both Krappé's formula (a) and Guet *et al.*'s formula (b) at $T = 3.3272$ MeV and $E_{\text{c.m.}} = 51.6$. ΔR is the same as in Fig. 6.

as to reproduce the experimental cross sections. Similarly, for IMFs the touching configuration is extended by the free parameter ΔR taking values of 0.82 and 0.84 fm corresponding to Krappé's formula and Guet *et al.*'s formula, respectively. In Fig. 6(a), the preformation probability value corresponding to the fragment ^1H has a large value at $\ell = 0\hbar$ onward, and it decreases as the ℓ value increases. For other light particles the preformation probabilities are too low and in this scale it is not showing any structural effect. The summed preformation probabilities of LPs goes to zero at an ℓ value of $38\hbar$ which is taken as ℓ_{max} in the calculations. In Fig. 6(a) the α -structured nuclei clearly exhibit structural effects. The fragment ^4He has large preformation probability values starting from $\ell = 0\hbar$ onward and they increase as the ℓ value increases and reach a maximum value around $25\hbar$, beyond this they start to decrease. For ^8Be the preformation probability values start to contribute after $15\hbar$ and increase with angular momentum and attaining a maximum around $30\hbar$ and beyond which they decrease. For the other α -structured nuclei, viz., ^{12}C to ^{28}Si , the preformation probability starts to contribute beyond $25\hbar$. For rest of the fragments the values are too low.

The use of Krappé's formula exhibits strong preformation for α -structured nuclei as a function of angular momentum. However, in Fig. 6(b), the calculations obtained with Guet *et al.*'s formula do not show any strong preformation for α -structured nuclei. The structural effects are present only for ^1H and ^{28}Si . The preformation probability is largest for ^1H

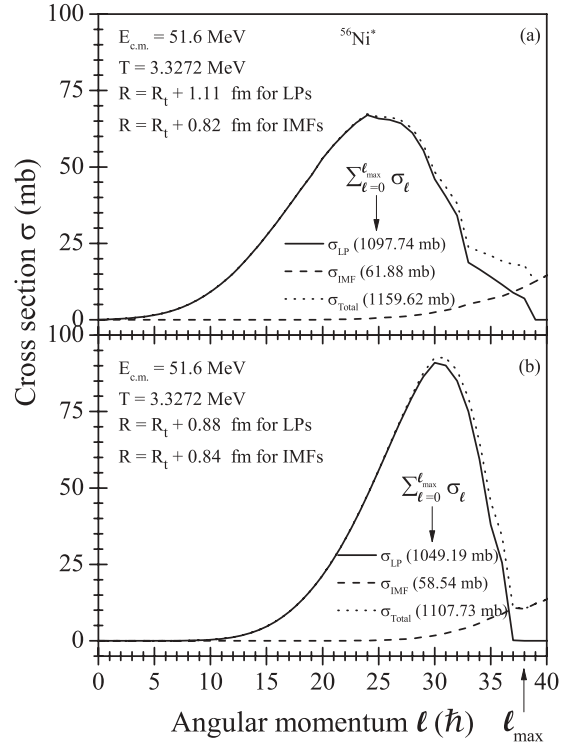


FIG. 8. Light particle cross sections σ_{LP} (solid line), intermediate mass fragment cross sections σ_{IMF} (dashed line), and their sum σ_{Total} (dotted line) are calculated for $^{56}\text{Ni}^*$ at fitted ΔR with ℓ summed using Krappé's formula (a) and Guet *et al.*'s formula (b), respectively.

and it starts to contribute from $\ell = 0\hbar$ onward and it decreases as the ℓ value increases. A similar variation is seen for ^2H but with small values. For ^{28}Si , the preformation probability starts to contribute beyond $30\hbar$. Similar results are seen for another temperature considered, $T = 3.5405$ MeV.

Since the cross section is a combined effect of preformation and penetration probability the variation of penetration probability as a function of angular momentum and fragment mass number is presented in Fig. 7. Figures 7(a) and 7(b) correspond to Krappé's formula and Guet *et al.*'s formula, respectively. The ΔR values are the same as those discussed in Fig. 6. In Fig. 7(a), the penetration probability starts to contribute beyond $\ell = 25\hbar$ for fragments with $A > 4$. For $A < 4$, the contribution starts from lower ℓ values, say starting from around $\ell = 5\hbar$ onward. In the preformation values as well as the penetration probability values ^4He overlaps very much with light particles. Thus, ^4He could compete with light particles at lower angular momentum states. Though the LPs penetration probabilities are higher than the IMFs at large ℓ values, the LPs have smaller preformation probabilities at these ℓ values and hence LPs would not compete with the emission of IMFs at large ℓ values. In Fig. 7(b), since the free parameter ΔR values for LPs and IMFs are very close to each other, we can hardly see any distinguishing division between LPs and IMFs as is seen in Fig. 7(a). The contribution of penetration probability starts beyond $\ell = 15\hbar$. Though the values are comparable at larger ℓ values, the combined effect of preformation and penetration probabilities will show whether

TABLE I. The calculated cross sections for each experimentally observed fragment corresponding to the two incident energies using Krappe's formula and Guet *et al.*'s formula are compared with the earlier results obtained from Davidson *et al.*'s formula [21] and the results of EHFm [11] and TSM [10]. Also presented are the average total kinetic energies of our calculations compared with experimental data [9]. Summed values of LPs, IMFs, and total cross sections obtained with Krappe's formula and Guet *et al.*'s, formula are compared with experimental results [9].

$E_{c.m.}$ (MeV)	A_2	Cross section (σ) (mb)						$\overline{\text{TKE}}$ (MeV)			$\sum_{\ell=0}^{\ell_{\max}} \sigma$ (mb)			
		Exp.	Krappe	Guet <i>et al.</i>	[21]	EHFM	TSM	Exp.	Krappe	Guet <i>et al.</i>	Exp.	Krappe	Guet <i>et al.</i>	
51.60	12	9.20	9.71	3.59	11.48	7.50	9.91	26.19	28.94	28.38				
	14	0.70	0.03	2.66	22.54	0.73	2.50	-	-	-				
	16	3.82	5.43	2.30	3.26	5.27	5.55	30.52	31.65	31.53	σ_{LP}	1080 ± 130	1097.74	1049.19
	18	0.30	0.14	2.13	2.55	0.27	1.55	-	-	-				
	20	1.62	3.39	1.25	0.79	0.91	3.91	35.50	34.29	33.85	σ_{IMF}	59 ± 12	61.88	58.54
	22	0.41	0.16	1.46	0.87	0.59	1.23	-	-	-				
	24	3.03	2.51	1.05	0.22	3.00	3.00	38.53	35.29	35.02	σ_{Total}	1139 ± 142	1159.62	1107.73
	26	0.90	0.10	0.84	0.14	1.68	1.05	-	-	-				
60.50	28	1.84	4.32	2.59	0.05	4.36	2.50	38.10	36.03	35.37				
	12	17.49	21.07	9.10	24.27	14.52	15.79	28.08	29.60	28.64				
	13	2.21	0.59	4.15	4.21	1.02	2.68	-	-	-				
	14	2.50	0.05	6.72	47.68	3.15	2.83	-	-	-				
	15	1.21	0.62	3.79	2.04	1.87	2.42	-	-	-				
	16	10.01	12.97	6.02	9.47	11.46	9.95	32.44	32.56	32.13				
	17	1.26	0.77	3.64	0.93	2.01	1.93	-	-	-	σ_{LP}	1050 ± 100	1059.34	1032.47
	18	1.84	0.37	5.92	8.17	2.24	2.39	-	-	-				
	19	1.26	0.70	3.63	0.87	0.64	1.35	-	-	-				
	20	5.57	8.87	3.54	3.71	3.65	7.06	35.00	35.08	34.60	σ_{IMF}	75.64 ^a	68.81	76.06
	21	1.48	0.73	3.93	0.99	1.02	1.33	-	-	-				
	22	2.47	0.45	4.29	3.90	2.99	2.20	-	-	-				
23	2.82	0.71	2.75	0.68	1.16	1.31	-	-	-	σ_{Total}	1125.64	1128.15	1108.53	
24	6.14	6.91	3.10	1.61	5.04	5.51	38.23	36.27	35.69					
25	4.27	0.62	2.16	0.43	2.17	1.29	-	-	-					
26	5.60	0.27	2.40	0.87	8.51	1.76	-	-	-					
27	3.33	1.08	3.14	0.37	3.02	1.27	-	-	-					
28	6.18	12.05	7.78	0.93	13.73	5.07	37.42	37.02	35.83					

^aThis data is extracted from Fig. 12 of Ref. [9].

really light particles can compete with emission of IMFs at larger ℓ values.

The combined effect of preformation and penetration probability can be seen in the cross-section calculations. In Fig. 8, we present the cross sections for LPs (σ_{LP}), IMFs (σ_{IMF}), and total cross sections ($\sigma_{Total} = \sigma_{LP} + \sigma_{IMF}$) in panels (a) and (b), corresponding to Krappe's formula and Guet *et al.*'s formula, respectively. The cross-section values are summed from $\ell = 0$ to ℓ_{\max} . In Fig. 8(a) corresponding to Krappe's formula, the cross section for LPs starts to contribute from very low ℓ values, say from $\ell = 5\hbar$ onward and it reaches a maximum value around $\ell = 25\hbar$ and starts to decrease with further increases in ℓ values. The results of Guet *et al.*'s formula presented in Fig. 8(b) show that the cross section for LPs starts to contribute beyond $\ell = 10\hbar$ and reaches a maximum value around $\ell = 30\hbar$ and decreases with increases in ℓ values. The cross section of IMFs starts to contribute beyond $\ell = 30\hbar$ in both cases and it increases with increases in ℓ values. The fission channels start to compete with LPs only at higher angular momentum states, a result already reflected in the potential energies presented in Figs. 4 and 5, respectively, for Krappe's formula and Guet *et al.*'s formula. To fit the

experimental cross section of LPs the neck length parameter $\Delta R = 1.11$ fm and $\Delta R = 0.88$ fm are used, respectively, for Krappe's formula and Guet *et al.*'s formula. However, fine tuning of this free parameter to reproduce the exact value of experimental data is not attempted. For the IMF cross section the neck length parameters $\Delta R = 0.82$ fm and $\Delta R = 0.84$ fm are used, respectively, for Krappe's formula and Guet *et al.*'s, formulas. Our calculated values, which are given in the legends within parentheses, are to be compared with the experimental values, viz., $\sigma_{LP} = 1080 \pm 130$ mb, $\sigma_{IMF} = 59 \pm 12$ mb, and $\sigma_{Total} = 1139 \pm 142$ mb. For the other energy at 60.5 MeV, our calculated values corresponding to σ_{LP} are 1059.34 and 1032.47 mb, respectively, for the use of Krappe's formula and Guet *et al.*'s formula and are to be compared with the experimental value of $\sigma_{LP} = 1050 \pm 100$ mb; these values are also listed in Table. I. Furthermore, for the incident energy $E_{c.m.} = 60.5$ MeV, the experimental $\sigma_{IMF} = 75.64$ mb, as shown in Table I, is the sum of cross sections for fragments from $A = 12$ to 28 whose values are taken from Fig. 12 of Ref. [9]. The corresponding calculated values using Krappe's formula and Guet *et al.*'s, formula are 68.81 and 76.06 mb, respectively, which are also the sums of cross sections for the

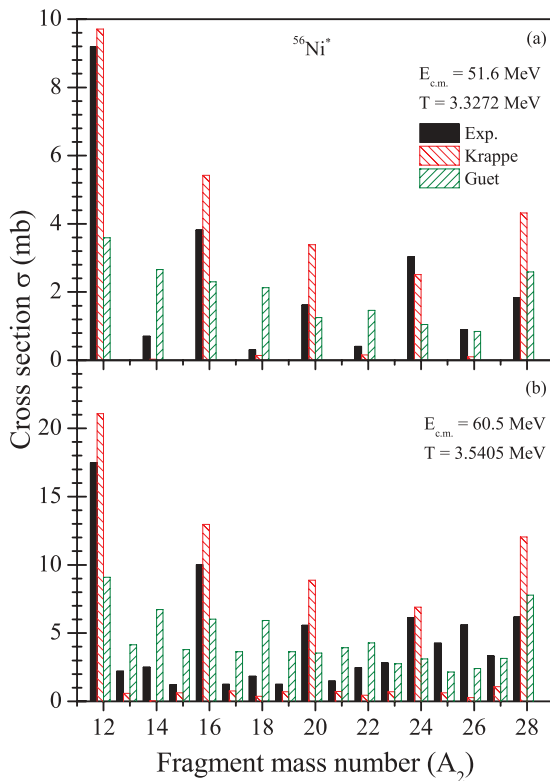


FIG. 9. (Color online) Histograms of the calculated IMF cross sections σ_{IMF} using Krappe's formula and Guet *et al.*'s formula are compared with the experimental data [9] at $E_{\text{c.m.}} = 51.6$ and 60.5 MeV in panels (a) and (b), respectively.

fragments from $A = 12$ to 28 . For IMFs the single parameter is used for all the fragments with mass numbers $A > 5$. Though this parameter reproduces the IMF cross section fairly well with experimental data, the calculated cross section for each channel however does not match well with that of the experimental values as is shown in Fig. 9.

In Fig. 9, for both the energies considered, we compare our calculated cross section for each channel with respect to the experimental data. In Figs. 9(a) and 9(b), corresponding to the energies $E_{\text{c.m.}} = 51.6$ and 60.5 MeV, the cross section for $A = 12$ to 28 (for 51.6 MeV only even mass fragments are observed [9], and for 60.5 MeV the odd mass fragments are also observed) are compared with our results. The results of Krappe's formula for both the energies considered exhibit a strong distribution of cross sections only for α -structured nuclei. For the rest of the fragments, the cross-section values predicted are at least lower by a factor of 2 to 3 compared with the experimental data as is seen from the numerical values presented in Table I. This may be due to the presence of strong minima in the potential valley for α nuclei as well as to strong preformation of α nuclei as presented in Figs. 4 and 6. However, the calculations obtained with Guet *et al.*'s formula though do not show any explicit preference for α -structured nuclei, but compare reasonably well with experimental data at least for some fragments. The cross section values for the non- α even- A fragments obtained with Guet *et al.*'s formula at both the energies decrease with an increase in mass number

except for a small hike at $A_2 = 22$ and a large value at $A_2 = 28$. For the odd- A fragments corresponding to the energy $E_{\text{c.m.}} = 60.5$ MeV similar results are also seen; however, for odd- A fragments the cross-section values are lower than those for even- A fragments.

Also given in Table I are the results from earlier work by one of us using Davidson's formula and the results of two other models EHFM [11] and TSM [9]. The average TKE values are calculated as the weighted average of the TKE with the weight factor taken as the ratio of each fragment cross section corresponding to each angular momentum and the total cross section. To fit with the experimental values, the ℓ value is varied and for Krappe's formula and Guet *et al.*'s formula the values are varied as follows: $\ell = 26\hbar$ and $\ell = 25\hbar$, respectively, for the energy 51.6 MeV and $\ell = 26\hbar$ and $\ell = 24\hbar$, respectively, for the energy 60.5 MeV. However, the value of the parameter ΔR remains the same as that used to reproduce the overall cross sections for the IMFs.

IV. SUMMARY

In summary, the DCM is used to study the role of temperature-dependent binding energies. For this the temperature-dependent binding energy formulas of Krappe and Guet *et al.* are used without any refitting of their coefficients. Due to the presence of terms like pairing and the Wigner term the Krappe formula reproduces very well the ground-state binding energies. The inclusion of the Wigner term for light nuclei resulted in a large deviation and hence is not considered for light nuclei with mass numbers up to $A = 11$. Due to the absence of pairing and Wigner terms in Guet *et al.*'s formula the ground-state binding energies are not reproduced well. However, at the temperatures that interest us these terms may not play a crucial role. Unlike in earlier works on the DCM, the calculated binding energies are used rather than the mass excess values. The temperature-dependent radius expression also is now considered to have a quadratic dependence on temperature which also differs from earlier works on the DCM.

This reformulated DCM is applied for the decay of hot and rotating $^{56}\text{Ni}^*$ compound systems formed in $^{32}\text{S} + ^{24}\text{Mg}$ at two different incident energies. The results obtained using Krappe's formula exhibit an explicit preference for α -structured nuclei which is reflected in the fragmentation potential energy, preformation calculations, and in the individual channel cross sections. The overall cross-section values for the LPs and IMFs as well as the individual channel cross sections for the α -structured nuclei compare well with experimental data. The calculations using Guet *et al.*'s formula though do not exhibit any strong structural effects in the results of fragmentation potential or preformation probability calculations; rather the results compare reasonably well with the overall experimental cross sections for the LPs and IMFs. The explicit preference for α structure is shown not to vanish with the inclusion of temperature and rather it is shown as the inherent property of the form of the binding energy formulas we use. Also it is shown that refitting of the coefficients of the original forms of the binding energy formulas is not required.

ACKNOWLEDGMENTS

One of the authors M.B. acknowledges financial support in the form of a project sanctioned to him by the University

Grants Commission of India, Grant No. 37-100/(2009). N.S.R. acknowledges support in the form of a study leave granted by the Avinashilingam Institute for Home Science and Higher Education for Women-University, Coimbatore.

-
- [1] S. J. Sanders, A. Szanto de Toledo, and C. Beck, *Phys. Rep.* **311**, 487 (1999).
- [2] N. V. Antonenko, S. P. Ivanova, R. V. Jolos, and W. Scheid, *Phys. Rev. C* **50**, 2063 (1994).
- [3] G. G. Adamian, N. V. Antonenko, and W. Scheid, *Phys. Rev. C* **68**, 034601 (2003).
- [4] Sh. A. Kalandarov, G. G. Adamian, N. V. Antonenko, W. Scheid, and J. P. Wieleczko, *Phys. Rev. C* **84**, 064601 (2011).
- [5] G. Adamian, N. Antonenko, and W. Scheid, in *Clusters in Nuclei*, Vol. 2, Lecture Notes in Physics, Vol. 848, edited by C. Beck (Springer, Heidelberg, 2012), p. 165.
- [6] G. Royer, C. Bonilla, and R. A. Gherghescu, *Phys. Rev. C* **67**, 034315 (2003).
- [7] R. A. Gherghescu and G. Royer, *Phys. Rev. C* **68**, 014315 (2003).
- [8] R. J. Charity *et al.*, *Nucl. Phys. A* **476**, 516 (1988); **483**, 371 (1988).
- [9] S. J. Sanders *et al.*, *Phys. Rev. Lett.* **59**, 2856 (1987); *Phys. Rev. C* **40**, 2091 (1989).
- [10] S. J. Sanders, *Phys. Rev. C* **44**, 2676 (1991).
- [11] T. Matsuse, C. Beck, R. Nouicer, and D. Mahboub, *Phys. Rev. C* **55**, 1380 (1997).
- [12] R. R. Betts, S. B. DiCenzo, and J. F. Petersen, *Phys. Rev. Lett.* **43**, 253 (1979); R. Nouicer *et al.*, *Phys. Rev. C* **60**, 041303 (1999); C. Beck, R. Nouicer, D. Disdier, G. Duchene, G. de France, R. M. Freeman, F. Haas, A. Hachem, D. Mahboub, V. Rauch, M. Rousseau, S. J. Sanders, A. Szanto de Toledo, *ibid.* **63**, 014607 (2000).
- [13] R. R. Betts and S. Saini, *Phys. Scr.* **1983**, 204 (1983).
- [14] B. K. Dichter, P. D. Parker, S. J. Sanders, R. R. Betts, and S. Saini, *Phys. Rev. C* **35**, 1304 (1987).
- [15] B. Shivakumar, S. Ayik, B. A. Harmon, and D. Shapira, *Phys. Rev. C* **35**, 1730 (1987).
- [16] B. Shivakumar, D. Shapira, P. H. Stelson, S. Ayik, B. A. Harmon, K. Teh, and D. A. Bromley, *Phys. Rev. C* **37**, 652 (1988).
- [17] R. K. Gupta, M. Balasubramaniam, C. Mazzocchi, M. La Commara, and W. Scheid, *Phys. Rev. C* **65**, 024601 (2002).
- [18] R. K. Gupta, R. Kumar, N. K. Dhiman, M. Balasubramaniam, W. Scheid, and C. Beck, *Phys. Rev. C* **68**, 014610 (2003).
- [19] M. Balasubramaniam, R. Kumar, R. K. Gupta, C. Beck, and W. Scheid, *J. Phys. G: Nucl. Part. Phys.* **29**, 2703 (2003).
- [20] R. K. Gupta, M. Balasubramaniam, R. Kumar, D. Singh, and C. Beck, *Nucl. Phys. A* **738**, 479 (2004).
- [21] R. K. Gupta, M. Balasubramaniam, R. Kumar, D. Singh, C. Beck, and W. Greiner, *Phys. Rev. C* **71**, 014601 (2005).
- [22] R. K. Gupta, M. Balasubramaniam, R. Kumar, D. Singh, S. K. Arun, and W. Greiner, *J. Phys. G: Nucl. Part. Phys.* **32**, 345 (2006).
- [23] B. B. Singh, M. K. Sharma, and R. K. Gupta, *Phys. Rev. C* **77**, 054613 (2008).
- [24] R. Kumar and R. K. Gupta, *Phys. Rev. C* **79**, 034602 (2009).
- [25] R. K. Gupta, Niyti, M. Manhas, and W. Greiner, *J. Phys. G: Nucl. Part. Phys.* **36**, 115105 (2009).
- [26] R. K. Gupta, in *Clusters in Nuclei*, Vol. 1, Lecture Notes in Physics, Vol. 818, edited by C. Beck (Springer, Heidelberg, 2010), p. 223.
- [27] Niyti, R. K. Gupta, and W. Greiner, *J. Phys. G: Nucl. Part. Phys.* **37**, 115103 (2010).
- [28] M. K. Sharma, G. Sawhney, R. K. Gupta, and W. Greiner, *J. Phys. G: Nucl. Part. Phys.* **38**, 105101 (2011).
- [29] K. Sandhu, M. K. Sharma, and R. K. Gupta, *Phys. Rev. C* **85**, 024604 (2012).
- [30] M. K. Sharma, S. Kanwar, G. Sawhney, and R. K. Gupta, *Phys. Rev. C* **85**, 064602 (2012).
- [31] N. J. Davidson, S. S. Hsiao, J. Markram, H. G. Miller, and Y. Tzeng, *Nucl. Phys. A* **570**, 61 (1994).
- [32] W. D. Myers and W. J. Swiatecki, *Nucl. Phys.* **81**, 1 (1966).
- [33] H. J. Krappe, *Phys. Rev. C* **59**, 2640 (1999).
- [34] C. Guet, E. Strumberger, and M. Brack, *Phys. Lett. B* **205**, 427 (1988).
- [35] M. Brack, *Phys. Rev. Lett.* **53**, 119 (1984).
- [36] M. Brack, C. Guet, and H. B. Haakansson, *Phys. Rep.* **123**, 275 (1985).
- [37] P. Möller, and J. R. Nix, *At. Data Nucl. Data Tables* **39**, 213 (1988).
- [38] G. Audi, A. H. Wapstra, and C. Thibault, *Nucl. Phys. A* **729**, 337 (2003).
- [39] J. Blocki, J. Randrup, and W. J. Swiatecki, and C. F. Tsang, *Ann. Phys. (NY)* **105**, 427 (1977).
- [40] H. Kröger and W. Scheid, *J. Phys. G: Nucl. Part. Phys.* **6**, L85 (1980).